

A Study on Efficient Electric Propulsion System

Jae-Jung HUR[†]

Korea Maritime and Ocean University(professor)

효율적인 전기추진시스템에 관한 연구

허재정[†]

한국해양대학교(교수)

Abstract

In this study, induction motors, which are often used in mid- to large-size ships owing to their durability and price competitiveness, are considered for small electric propulsion ships with space constraints and large-torque requirements. The proposed power conversion system is efficient for propulsion motors in constrained spaces, exhibits a low switching loss, and does not require a speed sensor. It uses an active front-end converter and an induced motor sensorless speed control method with current error compensation. A hysteresis controller was used for reducing the switching loss, and senseless speed control of the induction motor was performed using the current error compensation method. Computer simulation was performed using a PSIM program, and it was verified that the presented electric propulsion system has the same operating characteristics as the system to which a sensor is attached.

Key words : Electric propulsion ships, AFE Converter, Induction motor, Sensorless speed control

1. Introduction

Air pollution generated by ships is gradually increasing, constituting a global problem. To alleviate this problem, the International Maritime Organization has limited the sulfur content of ship fuels to 0.5% at the 70th MEPC meeting. At the 72nd MEPC meeting, short-term reduction goals (that should be met by 2030) and mid- to long-term reduction goals (that should be met by 2050) were set, for achieving the overall goal of

reducing the amount of greenhouse gas-related pollution. At the recently held 76th MEPC,

measures were proposed for reducing greenhouse gas emissions by considering their technical and operational aspects. To promote the distribution and development of eco-friendly ships, Korea also enacted the ‘Eco-friendly Ships Act’, which has been in effect since January 1, 2020. Accordingly, eco-friendly ship propulsion systems that can replace existing propulsion systems are actively considered. The development of electric propulsion ships as eco-friendly ship propulsion systems is also proceeding.

In the case of a large merchant ship equipped with an electric propulsion device, various

[†] Corresponding author: 0108512-0571, jjheo@kmou.ac.kr/orcid.org/0000-0002-0519-7717

* This study was conducted with the support of Korea Maritime University's 2020 second half of 2020 new professor settlement research support project.

harmonic-reducing devices, such as phase-shift transformers, have been installed for reducing switching losses by easily securing space (Abu-Rub, 2013; Steinke, 1999). However, in the case of small leisure boats or fishing boats, it is difficult to procure necessary space for a power conversion system; moreover, there is a limited ability to install devices for cooling the heat generated during switching. Therefore, in small ships, active front-end converters have been the easiest to install among the various devices for reducing harmonics (Hur, 2020; Hur et al., 2018). Various studies have been conducted for reducing the switching loss, which is one of the disadvantages of power conversion systems. To this end, various current control methods have been used, which do not cause significant switching and have excellent transient response characteristics (Kim, 2016). Among them, the hysteresis control method is the most useful for small systems, owing to its simplicity of operation (Hur, 2020; Jeong et al., 2003).

Alternating current (AC) motors use vector control and direct torque control techniques for achieving high performance (Lee et al., 2000). While vector control is used in various industrial fields, in the direct torque control approach, the control target is not the speed; thus, the speed of the motor is determined by the applied load. The direct torque control method is widely used in control applications, where space is constrained and large-capacity torque is required, such as for electric railways.

To stably control the speed of the induction motor without a speed sensor, various sensorless speed control methods have been used (Wlas et al., 2005; Kim et al., 2012). Among these sensorless speed control methods, the current error

compensation method is arguably the simplest and the best control method (Hur et al., 2021).

Although inexpensive and durable induction motors have been used in large and medium-sized ships, permanent magnet synchronous motors have been widely used in small ships, owing to their advantages such as high efficiency, high power factor, and high power density. However, recently, the application of induction motors to small ships has been attempted.

This paper presented a power conversion system with an induction motor sensorless control method using an AFE converter with a hysteresis controller with high utilization of space and low switching loss, to control the propulsion motor speed of small ships. The validity of the presented system was confirmed through a computer simulation.

II . Materials and Methods

1. Electric propulsion system

The general electric propulsion system used in electric propulsion ships is shown in [Fig. 1].

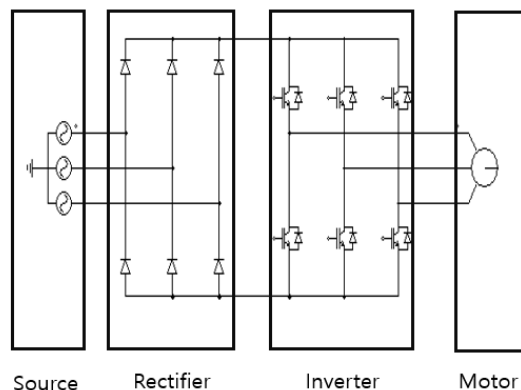


[Fig. 1] General electric propulsion system.

The electric propulsion system consists of a

source unit that supplies three-phase power, a rectifier stage that converts AC to DC, an inverter stage that controls the AC motor for propulsion, and a propulsion motor.

2. AFE Rectifier

The AFE rectifier converts the power of the rectifier by controlling the phase and magnitude of the AC input current, and adjusts the input current by controlling the rectifier input voltage. The rectifier input voltage controls the frequency, voltage, and phase, but the frequency must be the same as that of the power supply's voltage, so that the voltage and the phase are controlled.

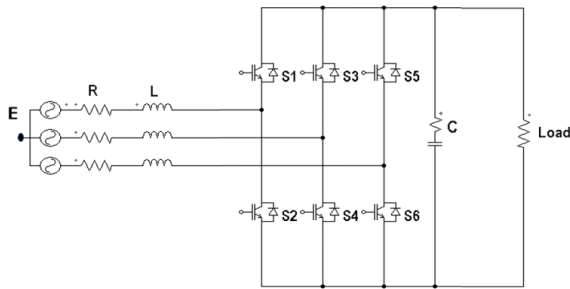


[Fig. 2] Circuit diagram of AFE rectifier.

That is, when the magnitude of the phase angle increases and the input voltage increases, the magnitude of the input current should increase as well. In this way, the device operates in the rectification mode while maintaining an excellent power factor.

[Fig. 2] shows a three-phase AFE rectifier. The rectifier is composed of six switches in three stages, and a capacitor is installed on the direct current (DC) side, to maintain a constant DC output voltage despite sudden voltage fluctuations. To control the magnitude of the rectifier's input current during power conversion, an inductor is

installed on the power output side. The AC power sources e_a , e_b , e_c maintain a three-phase equilibrium.

When the switches of the upper and lower parts are turned on simultaneously, dv/dt increases rapidly and damages the switch; therefore, when the switches are operated, the delay time is set such that the two switches are turned on and off.

$$e_a + e_b + e_c = 0 \dots\dots\dots (1)$$

$$i_a + i_b + i_c = 0 \dots\dots\dots (2)$$

The voltage equation of the rectifier is

$$e_a = Ri_a + L \frac{di_a}{dt} + V_a \dots\dots\dots (3)$$

$$e_b = Ri_b + L \frac{di_b}{dt} + V_b \dots\dots\dots (4)$$

$$e_c = Ri_c + L \frac{di_c}{dt} + V_c \dots\dots\dots (5)$$

where e_a , e_b and e_c are the supply voltages of the a, b, and c phases, respectively, i_a , i_b , i_c are the phase currents, while V_a , V_b , V_c are the rectifier input voltages.

2. Direct torque control

The direct torque control method calculates the torque and the stator flux by measuring the voltage and current values in the motor. In addition, the torque error and the magnetic flux error are, respectively, provided to a hysteresis controller by comparing them with the command values of the magnetic flux and torque at every cycle. The output of the hysteresis controller is used as an input to a look-up table of voltage vectors, where

a desired voltage vector is found and output.

Direct torque control is advantageous owing to its fast response and accuracy, because it independently controls the magnetic flux and the torque. In addition, control precision and the switching frequency may be varied by adjusting the hysteresis bandwidth using the errors of the magnetic flux and torque as inputs. The control structure is very simple in the digital form, and the dynamic characteristics of the torque only weakly affect the parameter variation of the motor rotor, while affording computational efficiency.

However, there are disadvantages in that the switching frequency is variable, and many ripples may occur in the torque and speed values. The control characteristics may deteriorate when the torque command is changed in the low-speed range and during start-up.

The stator flux can be expressed by Equation (6), using the voltage equation of the induction motor in the three-phase stationary coordinate system:

$$V = RI + \frac{d}{dt} \lambda \dots\dots\dots (6)$$

If the value of the stator magnetic flux is obtained from Equation (6), it is incorporated into Equation (7):

$$\begin{aligned} \lambda_s &= \int (v_s - R_s i_s) dt \\ &= V_s \cdot t - R_s \int i_s dt \\ &= \frac{2}{3} V_{dc} [S_a + S_b e^{j\frac{2\pi}{3}} + S_c e^{j\frac{4\pi}{3}}] \cdot t \\ &\quad - R_s \int i_s dt + \lambda_s |_{t=0} \dots\dots\dots (7) \end{aligned}$$

Here, V_{dc} is the DC link voltage.

In Equation (7), because the stator resistance value is very small, if we assume that the voltage drop $R_s i_s$ is very small compared with the first equation and ignore it, the stator flux becomes proportional to the magnitude of the stator voltage and can be considered as a vector in the same direction.

The above relationship is captured by Equation (8), as follows:

$$\Delta \lambda_s \approx V_s \Delta t \dots\dots\dots (8)$$

where Δt is the sampling period.

In other words, the stator flux moves in the same direction as the stator voltage vector V_s . When V_s is an effective vector, λ_s moves at a constant rate with the output voltage vector of the inverter, and when it is an ineffective vector, it moves at a very low speed. Accordingly, the rotational speed of the magnetic flux is controlled by the ratio of the effective and ineffective vectors of the inverter output voltage vector.

<Table 1> lists the voltage vectors selected when the stator magnetic flux is in the n-th sector.

The magnetic flux and the torque selection direction of the motor are determined according to the eight voltage vectors that are output by the inverter, and by the current magnetic flux vector. The switching vector is selected by considering the magnitude of the magnetic flux and its direction.

[Fig. 3] is a conceptual diagram of the direct torque control, showing the switching vector and the magnetic flux vector.

<Table 1> Selected vector and definition

Vector	Definition
\mathbf{V}_n	Radial positive voltage vector
\mathbf{V}_{n+1}	Forward positive voltage vector
\mathbf{V}_{n+2}	Forward negative voltage vector
\mathbf{V}_{n+3}	Radial negative voltage vector
\mathbf{V}_{n-1}	Backward positive voltage vector
\mathbf{V}_{n-2}	Backward negative voltage vector
\mathbf{V}_0	Zero voltage vector

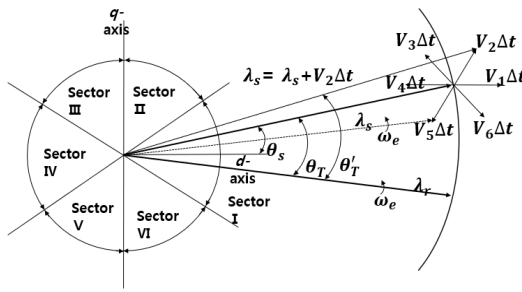


[Fig. 3] Conceptual diagram of the direct torque control method.

[Fig. 4] shows the trajectory of the rotating magnetic flux according to the selection of the switching vector in the hysteresis band. The magnetic flux rotates while drawing the trajectory of a pulsating circle, as shown in [Fig. 4].

Equation (9) describes the hysteresis band of the magnetic flux:

$$\left(|\lambda_s^*| - \Delta |\lambda_s| / 2 \right) \leq (|\lambda_s|) \dots\dots (9) \\ \leq \left(|\lambda_s^*| + \Delta |\lambda_s| / 2 \right)$$

The selection of the magnetic flux vector is not only related to the magnitude within the hysteresis band, but also to the direction of rotation.

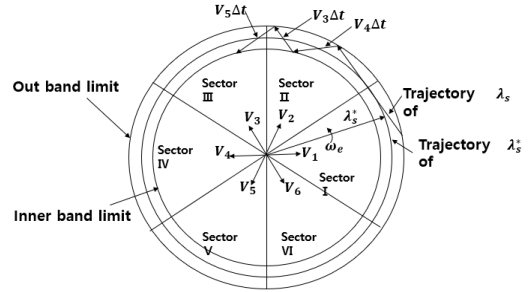


[Fig. 4] Trajectories of the reference λ_s^* with $x_T = 1$ and stator flux λ_s

For example, when the magnetic flux rotates clockwise, \mathbf{V}_6 is selected when the magnetic flux contacts the lower limit of the hysteresis band, while \mathbf{V}_5 is selected when it contacts the upper limit of the hysteresis band.

Similarly, when rotating counterclockwise, \mathbf{V}_2 and \mathbf{V}_3 are selected. When the magnetic flux is determined, the torque is determined using Equation (10):

$$T_e = \frac{3P}{2} \frac{L_m}{\sigma L_s L_r} |\lambda_s| |\lambda_r| \sin\theta_T \dots\dots (10)$$

When the torque value T_e reaches the setpoint T_e^* , T_e should decrease as slowly as possible to reduce the switching frequency of the inverter. That is, it is better to use an ineffective vector among the switching vectors of the inverter. The torque can be divided into two categories, according to the direction of the rotation.

$$T_e^* - \Delta T_e \leq T_e \leq T_e^* \\ \text{when } \lambda_s \text{ rotates clockwise}$$

$$T_e^* \leq T_e \leq T_e^* + \Delta T_e$$

when λ_s rotates counterclockwise

Assuming that λ_s rotates clockwise, when T_e touches T_e^* , an invalid vector is selected to stop the effective vector and reduce T_e .

Conversely, when T_e touches $T_e^* - \Delta T_e$ an effective vector for rotating the magnetic flux in the clockwise direction is selected.

To calculate the optimal voltage vector from <Table 2>, it is necessary to know the position information of the stator flux linkage. This positional information can be obtained from the values of the α axes and β axes of the stator flux linkage in the stationary coordinate system using Equations (11a), (11b) and (11c), as follows:

$$\begin{aligned} \lambda_s &= \lambda_{\alpha s} + j \lambda_{\beta s} \\ &= \int (v_{\alpha s} - R_s i_{\alpha s}) dt \\ &\quad + j \int (v_{\beta s} - R_s i_{\beta s}) dt \dots\dots\dots (11a) \end{aligned}$$

$$|\lambda_s| = \sqrt{\lambda_{\alpha s}^2 + \lambda_{\beta s}^2} \dots\dots\dots (11b)$$

$$\theta_s = \tan^{-1} \left(\frac{\lambda_{\beta s}}{\lambda_{\alpha s}} \right) \dots\dots\dots (11c)$$

Here, $v_{\alpha s}$, $v_{\beta s}$, $i_{\alpha s}$, $i_{\beta s}$ are the measured stator currents and voltages, respectively

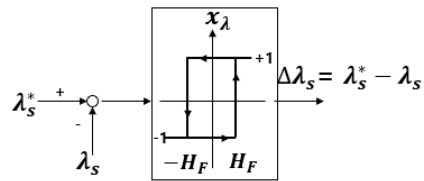
Therefore, the torque can be expressed as Equation (12), as follows:

$$T_e = \frac{3}{2} \frac{P}{2} (i_{\beta s} \lambda_{\alpha s} - i_{\alpha s} \lambda_{\beta s}) \dots\dots\dots (12)$$

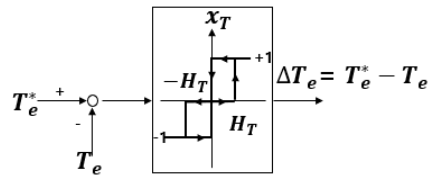
[Fig. 5(a)] shows the magnetic flux hysteresis controller. In the case of the stator magnetic flux, because the magnitude of the magnetic flux is

always positive, the comparator output $\Delta |\lambda_s|$ consists of two steps (1,-1). That is, when the stator flux error is larger than the positive hysteresis band H_F , it becomes $\Delta |\lambda_s| = 1$, and when the stator flux error is smaller than the negative hysteresis band $-H_F$, it becomes $\Delta |\lambda_s| = -1$

[Fig. 5(b)] shows the torque hysteresis controller used in the inverter of the direct torque control method. In general, unlike a magnetic flux hysteresis comparator, output ΔT_e is in three stages (-1, 0, 1) so that both forward and reverse torque commands can be followed.



(a) Flux Comparator



(b) Torque Comparator

[Fig. 5] Characteristics of torque and flux hysteresis comparator.

<Table 2> shows the lookup table of the optimal switching voltage vector based on the characteristics of the magnetic flux and torque hysteresis comparator.

<Table 2> Optimum switching voltage vector look-up table

Comparat or Output		Sector					
x_λ	x_T	I	II	III	IV	V	VI
+1	+1	\mathbf{V}_2	\mathbf{V}_3	\mathbf{V}_4	\mathbf{V}_5	\mathbf{V}_6	\mathbf{V}_1
+1	0	\mathbf{V}_0	\mathbf{V}_0	\mathbf{V}_0	\mathbf{V}_0	\mathbf{V}_0	\mathbf{V}_0
+1	-1	\mathbf{V}_6	\mathbf{V}_1	\mathbf{V}_2	\mathbf{V}_3	\mathbf{V}_4	\mathbf{V}_5
-1	+1	\mathbf{V}_3	\mathbf{V}_4	\mathbf{V}_5	\mathbf{V}_6	\mathbf{V}_1	\mathbf{V}_2
-1	0	\mathbf{V}_0	\mathbf{V}_0	\mathbf{V}_0	\mathbf{V}_0	\mathbf{V}_0	\mathbf{V}_0
-1	-1	\mathbf{V}_5	\mathbf{V}_6	\mathbf{V}_1	\mathbf{V}_2	\mathbf{V}_3	\mathbf{V}_4

3. Sensorless speed control by current error compensation

If Equation (13) is shown as a differential equation with respect to the current, Equation (14) is obtained, as follows:

$$\begin{bmatrix} v_{\alpha s} \\ v_{\beta s} \\ v_{\alpha r} \\ v_{\beta r} \end{bmatrix} = \begin{bmatrix} R_s + pL_s & 0 & pL_m & 0 \\ 0 & R_s + pL_s & 0 & pL_m \\ pL_m & \omega_r L_m & R_r + pL_r & \omega_r L_m \\ -\omega_r L_m & pL_m & -\omega_r L_r & R_r + pL_r \end{bmatrix} \begin{bmatrix} i_{\alpha s} \\ i_{\beta s} \\ i_{\alpha r} \\ i_{\beta r} \end{bmatrix} \dots (13)$$

Here, p is a differential operator.

If Equation (13) is shown as a differential equation with respect to current, Equation (14) is obtained.

$$\begin{bmatrix} i_{\alpha s} \\ i_{\beta s} \\ i_{\alpha r} \\ i_{\beta r} \end{bmatrix} = \frac{1}{D} \begin{bmatrix} -L_r R_s & L_m^2 \omega_r & L_m R_r & L_m L_r \omega_r \\ -L_m^2 \omega_r & -L_r R_s - L_m L_r \omega_r & L_m R_r & \\ L_m R_s & -L_s L_m \omega_r & -L_s R_r & -L_s L_r \omega_r \\ L_s L_m \omega_r & L_m R_s & L_s L_r \omega_r & -L_s R_r \end{bmatrix} \begin{bmatrix} i_{\alpha s} \\ i_{\beta s} \\ i_{\alpha r} \\ i_{\beta r} \end{bmatrix} + \begin{bmatrix} L_r & 0 & -L_m & 0 \\ 0 & L_r & 0 & -L_m \\ -L_m & 0 & L_s & 0 \\ 0 & -L_m & 0 & L_s \end{bmatrix} \begin{bmatrix} v_{\alpha s} \\ v_{\beta s} \\ v_{\alpha r} \\ v_{\beta r} \end{bmatrix} \dots (14)$$

Here, $D = L_s L_r - L_m^2$

The generated torque and rotational speed of the motor are expressed by Equations (15) and (16), respectively, as follows:

$$T_e = \frac{3}{2} \frac{P}{2} (i_{\beta s} \lambda_{\alpha s} - i_{\alpha s} \lambda_{\beta s}) \dots (15)$$

$$p\omega_r = \frac{1}{J} (T_e - T_L - B\omega_r) \dots (16)$$

Here, $p\lambda_{\alpha s} = v_{\alpha s} - R_s i_{\alpha s}$

$p\lambda_{\beta s} = v_{\beta s} - R_s i_{\beta s}$

P is the number of poles, J and B are friction coefficient and the moment of inertia, respectively, and T_L is the load torque.

[Fig. 6] shows the block diagram of the sensorless speed control mechanism of the induction motor, presented in this study

The induction motor sensorless control system operates as follows:

(1) The phase voltage applied in the previous control loop, the motor phase current of two phases, and the DC link voltage are measured.

(2) By converting the voltage and current values into 3-phase/2-phase, the actual motor-generated torque and the magnitude and direction of the stator magnetic flux are calculated.

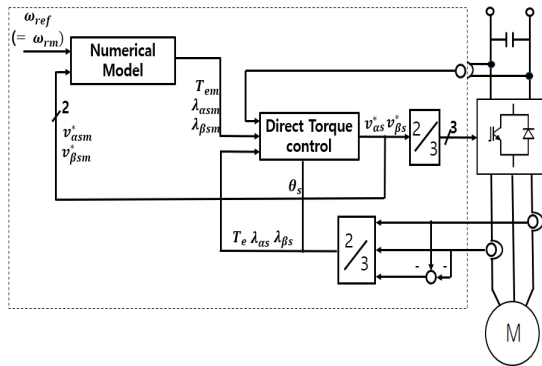


[Fig. 6] Block diagram of the proposed current error compensation control system for induction motors.

(3) The magnitudes of the model flux and torque are calculated using the phase voltage and the speed-setting value applied to the numerical model.

(4) After finding a sector by the stator magnetic flux direction obtained in (b), the optimal voltage vector is selected and output to the motor and model, so that the torque and magnitude of the magnetic flux of the actual motor approach the values of the numerical model.

(5) Since the same voltage is applied to the both sides to match the magnetic flux and torque of the motor and the numerical model, the speed of the motor is also given by Equations (14) and (15).

III. Results and Discussion

1. Simulation

In the high-speed and low-speed ranges, the speed control algorithm of an induction motor with a sensor attached to a general rectifier and the sensorless speed control method of an induction motor based on the AFE converter and current error compensation presented in this paper is comparatived using PISM software. In the computer simulation, first, a load proportional to the speed

square in the high-speed range (1,200 [rpm]) was applied, a step torque load was applied at 500 [rpm] in the low-speed range, and a forward/reverse operation was performed at 300 [rpm].

The system constants and parameters of the induction motor used in the computer simulation (<Table 3>).

<Table 3> Parameters of induction motor.

Rated output	4.2[kW]	R_r	2.2[Ω]
Rated voltage	220[V]	L_s	180[mH]
Rated current	12[A]	L_r	180[mH]
Rated speed	1,760[rpm]	L_{mr}	178 [mH]
Poles	4	J (Moment of inertia)	0.01[Kg·m ²]
R_s	2.2[Ω]	Sampling cycle	100[μs]

[Fig. 7] shows the PSIM block diagram of the direct torque control method induction motor driving simulation using the proposed AFE converter and the current error compensation senseless control method.

2. Simulation of an induction motor with a sensor attached.

[Fig. 8] shows the speed response characteristics of the induction motor when the speed command is applied from 0[rpm] to 1,200[rpm].

(a) shows the speed change of the motor, (b) shows the load change proportional to the speed square, and stable and stable control results are shown. (c) shows the input phase current in the steady state section, and the harmonic is 510 [%]. d) is the motor load current in the steady state section. (f) shows the input current and input voltage in the steady state section, and the power factor was 79.6 [%].

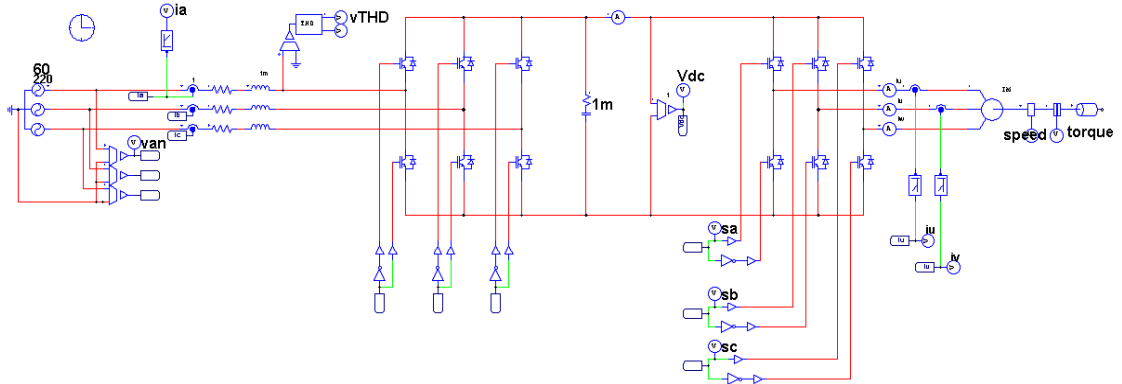
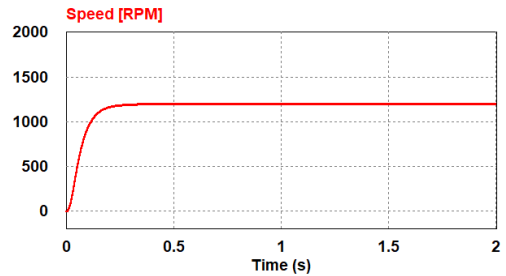


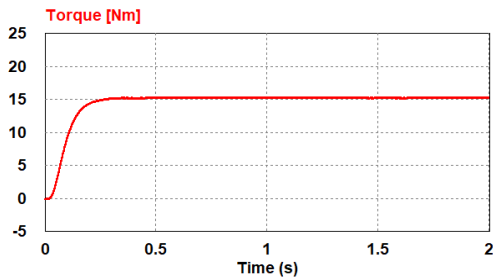
[Fig. 7] PSIM diagram of AFE converter and inverter.

[Fig. 9] shows the response state when a load torque of 5 [N m] is applied during steady state operation at 500 [rpm].

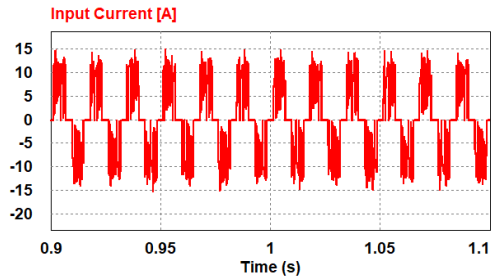
The motor speed change (a) and the torque change (b) before and after the application of the load torque reacted quickly. (c) shows the change in the phase current shape of the input stage before and after the application of the load torque,



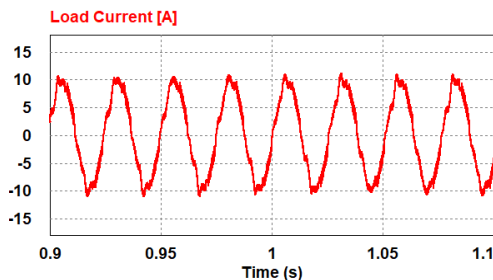
(a) Speed



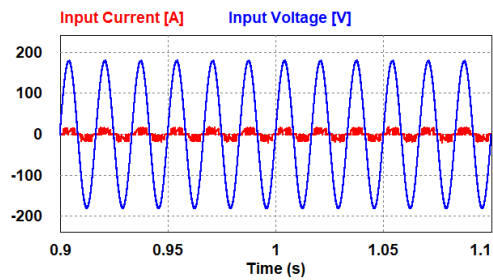
(b) Torque



(c) Input current



(d) Load current



(e) Power factor

[Fig. 8] Response characteristics according to speed change (0→1,200[rpm]).

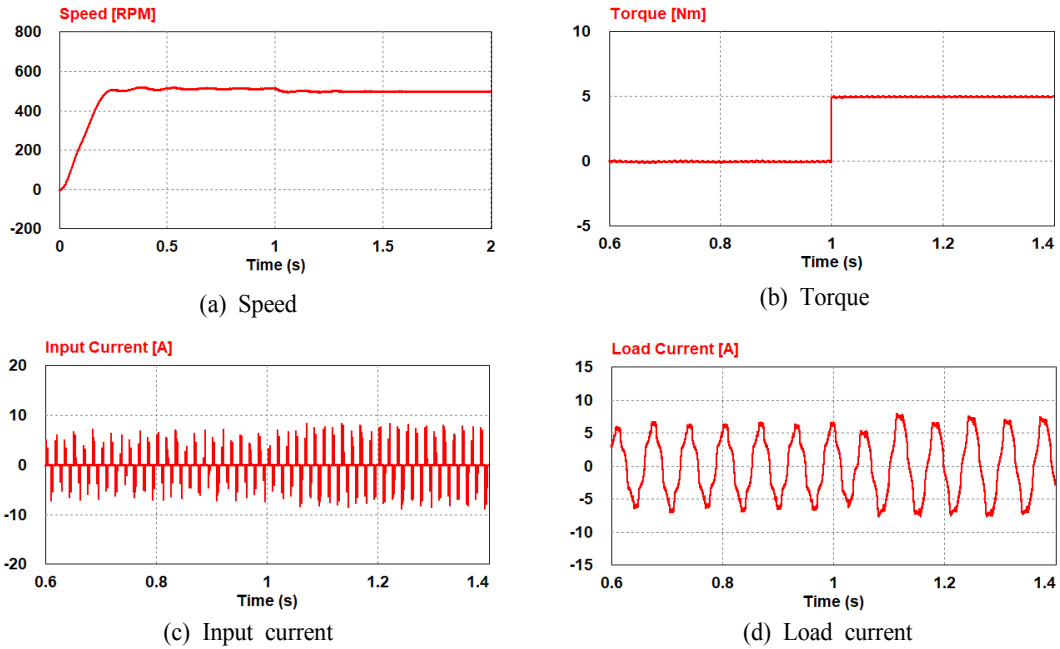


[Fig. 9] Response characteristics according to load torque change(500[rpm], 5[N·m]).

and the maximum load was increased from 7.2[A] to 8.9[A]. (d) shows the motor load current before and after the application of the load torque, and the current was stably controlled within 0.2 seconds.

[Fig. 10] shows the characteristics of the motor when the reverse speed command is applied at -300[rpm] while driving at 300[rpm]. (a) shows the speed change of the motor, and (b) shows the torque change before and after the application of the reverse speed command. Stable control results were shown when the reverse speed command was applied. (c) shows the change in the shape of the phase current at the input stage before and after applying the inversion command, and the current was stabilized within 0.2 seconds. (d) shows the motor load current before and after the reversal command, and according to the speed change, the load current was stably controlled within 0.2 seconds.

3. Simulation using AFE method and sensorless method

[Fig. 11] shows the speed response characteristics of the induction motor when a load proportional to the speed square was applied, and a speed command was applied from 0 to 1,200 [rpm]. (a) shows the speed change of the motor, and the stable speed control results are shown. (b) shows the load change proportional to the speed square, with a load shape similar to the speed change in the transient state. (c) shows the input phase current in the steady state, with a stable waveform close to a sine wave. (d) shows the motor load current in the steady state. (e) shows the voltage of the DC link and stably maintains the regulated voltage suitable for the AFE characteristics. (f) shows the input current and input voltage in the steady state, and a high power factor, at 99.4[%].

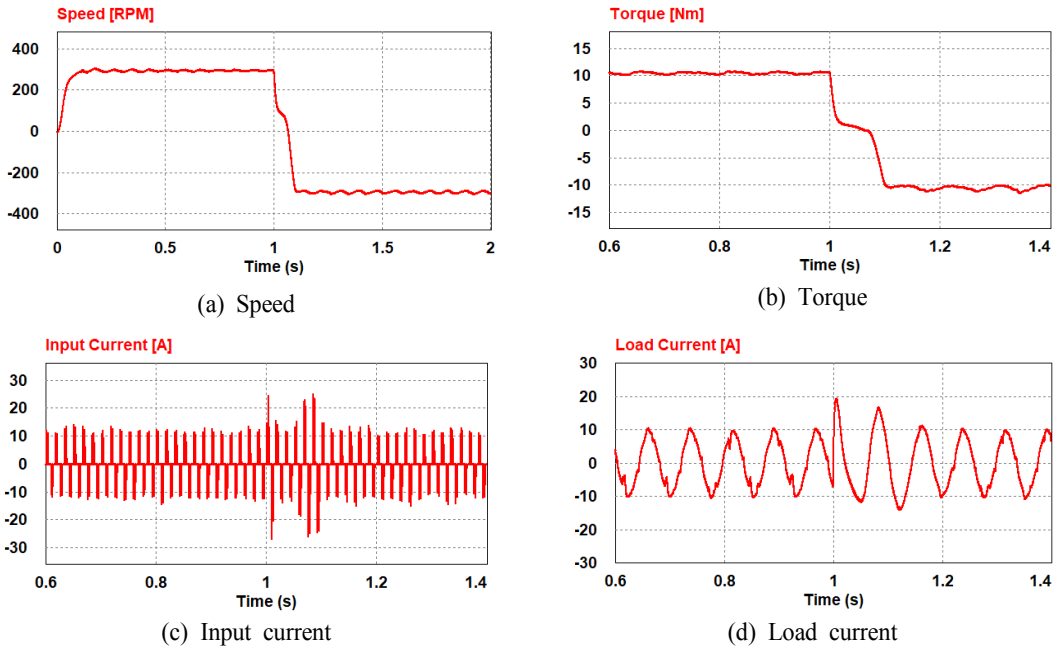


[Fig. 10] Response characteristics according to speed change(300 → -300 [rpm]).

[Fig. 12] shows the response state when a load torque of 5 [N·m] was administered during operation at 500 [rpm]. (a) shows the speed change of the motor, with stable control after the load application. Panel (b) shows the torque change, before and after the load torque. (c) shows the change in the shape of the input phase, the phase current before and after the load torque, and the input current with a shape close to that of a sine wave after the load stabilization. (d) shows the motor load current before and after the application of the load torque, and the current was stably controlled within 0.3 seconds.

[Fig. 13] shows the characteristics of the motor when a load proportional to the speed square was applied, and a reverse speed command was applied at -300 [rpm] while driving at 300 [rpm]. (a) shows the speed change of the motor, and shows

stable control results after the reverse speed command was applied. (b) shows the torque change before and after the application of the reversing speed command. It can be seen that it appears in a form similar to the speed change of the motor. (c) shows the change in the phase current shape of the input stage before and after application of the inversion command, and the current stabilized after 0.2 seconds. (d) shows the motor load current before and after the reversal command, and the load current was stably controlled after 0.2 seconds according to the speed change. current in the steady state. (e) shows the voltage of the DC link and stably maintains the regulated voltage suitable for the AFE characteristics. (f) shows the input current and input voltage in the steady state, and a high power factor, at 99.4[%].

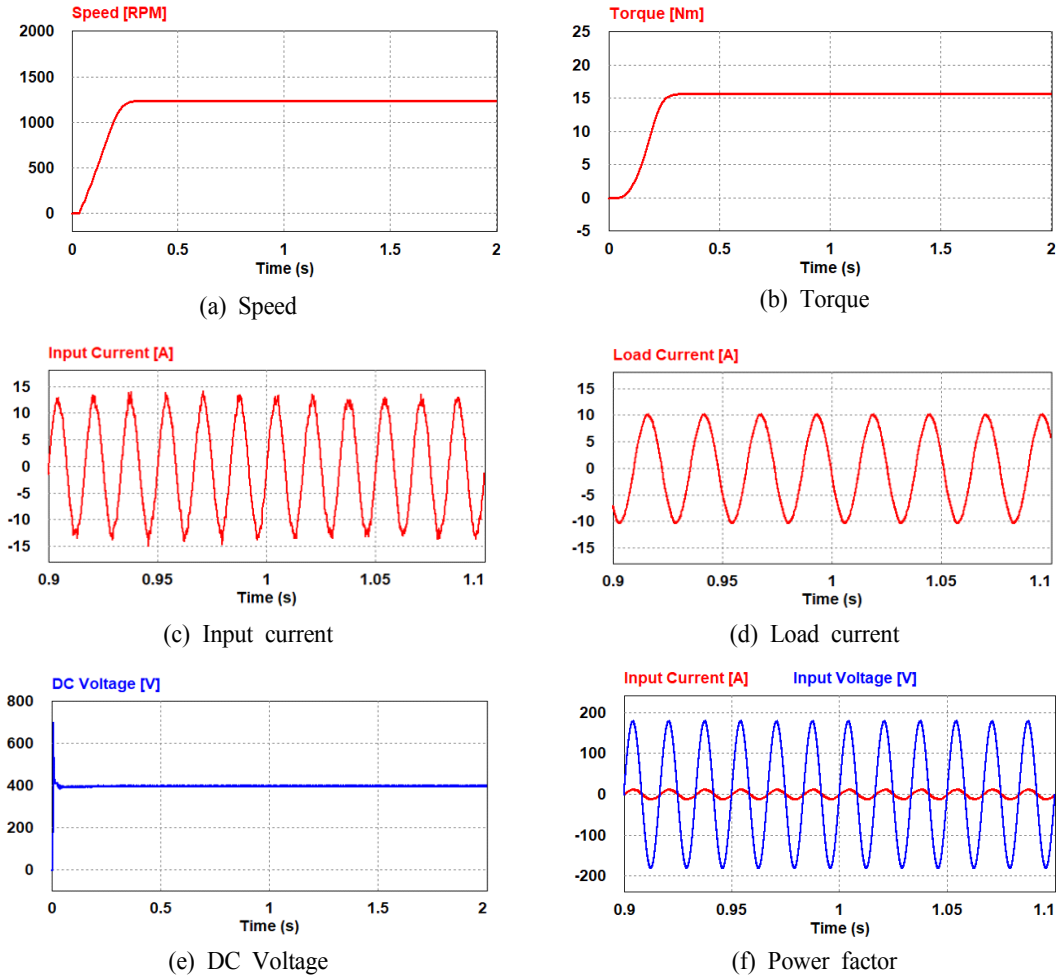


[Fig. 11] Response characteristics according to speed change (0→1,200[rpm]).

4. Review simulation results

When comparing [Fig. 8(a)], [Fig. 11(a)] and [Fig. 8(b)], [Fig. 11(b)] respectively, speed command is applied from 0[rpm] to 1,200[rpm], speed and torque are controlled stably. When comparing [Fig. 8(c)] and [Fig. 11(c)], the THD of the conventional method is 510[%] and presented method THD 7.97[%] shows a current waveform close to the sine wave, indicating that the input current is very good quality. When comparing [Fig.

8(d)] and [Fig. 11(d)], the maximum load current was about 10.5 [A] in the steady state section, and it was the same in both methods. In [Fig. 8(e)], the power factor was 79.6 [%], and in [Fig. 11(f)], it was found to be 99.4 [%] according to the characteristics of the AFE rectifier with improved power factor. In [Fig. 11(e)], a DC voltage of 400[V] can be obtained from an input current of AC 220[V] according to the characteristics of the AFE rectifier that can adjust the voltage.

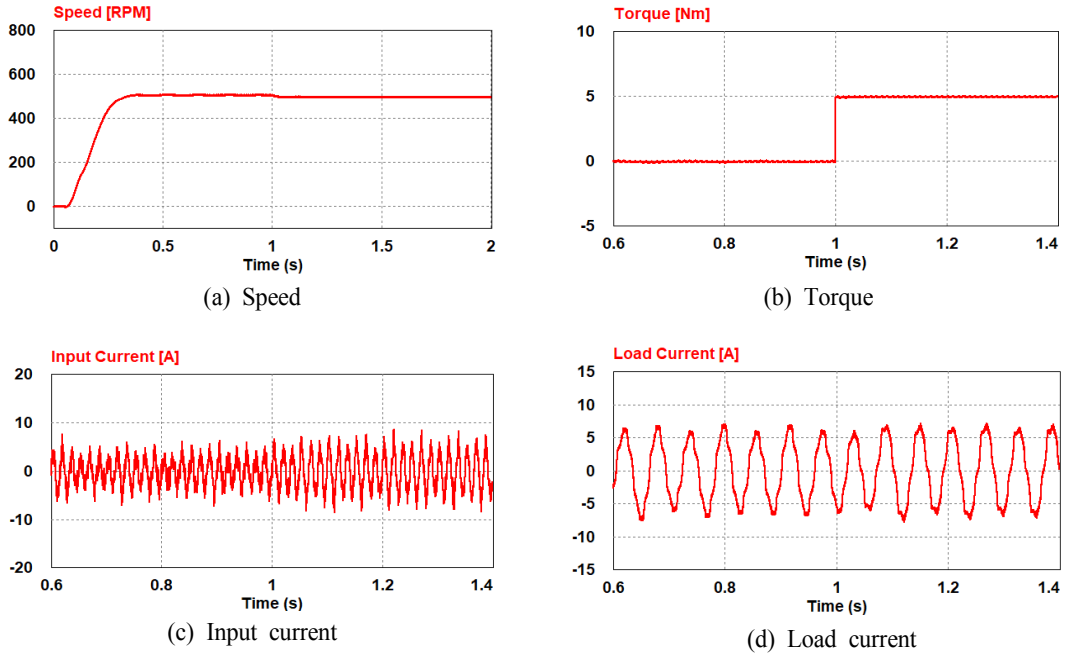


[Fig. 12] Response characteristics according to load torque change(500[rpm], 5[N·m]).

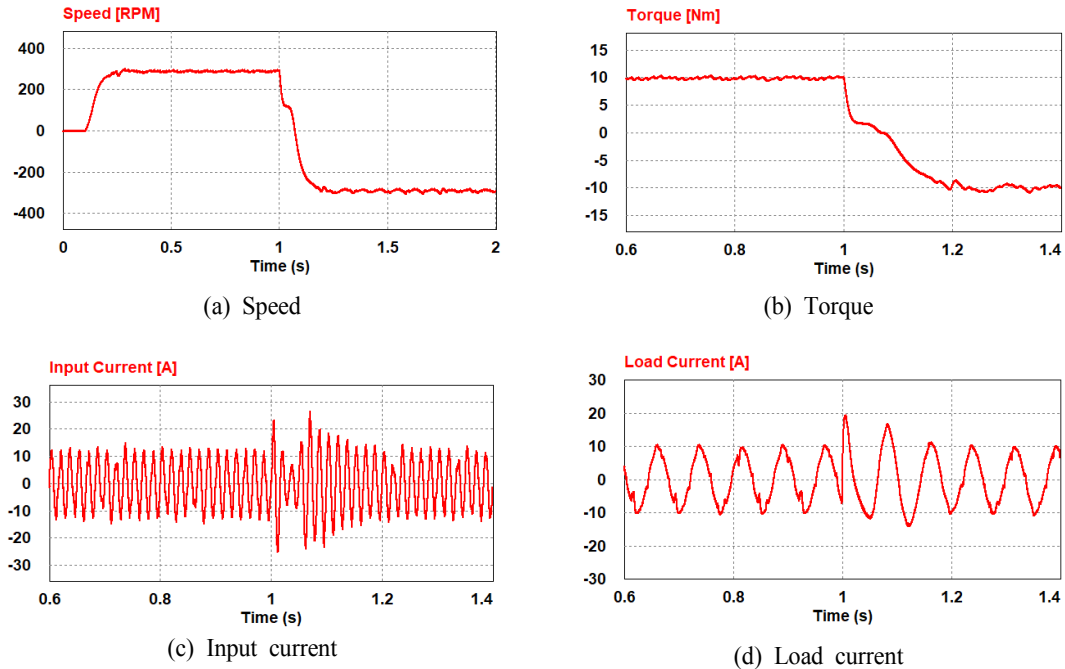


[Fig. 13] Response characteristics according to speed change(300 → -300 [rpm]).

When a load of 5 [N m] was applied while driving at 500 [rpm], comparing [Fig. 9(a)], [Fig. 12(a)] and [Fig. 9(b)], [Fig. 12(b)] showed stable speed and torque changes in both. In [Fig. 9(c)], [Fig. 9(d)] and [Fig. 12(c)], [Fig. 12(d)] after torque is applied, the input current and load current are stabilized after 0.15 seconds in the conventional method and after 0.2 seconds in the proposed method. At this time, the input current changes from 7.2[A] to 8.9[A] based on the maximum value. When a reverse command is applied during operation at 300[rpm], comparing [Fig. 10(a)], [Fig. 13(a)] and [Fig. 10(b)], [Fig. 13(b)] the speed and load were stabilized in 0.15 seconds in the conventional method, and the speed and load were stably controlled after 0.2 seconds in the proposed method. In [Fig. 10(c)], [Fig. 10(d)] and [Fig. 13(c)], [Fig. 13(d)] when the motor reverses, the input current and the load current are the same. The existing method stabilizes after 0.2 seconds and the proposed method after 0.25 seconds.

IV. Conclusion

In order to verify the performance of the converter using the active front-end rectification method and the senseless speed control of the induction motor applying the current error correction method, the existing method and the presented method were simulated using the PSIM program.

In the presented method, the AFE rectifier was able to obtain the optimal DC voltage through switching and the power factor was improved from 79.6[%] to 99.4[%]. The harmonics included in the input current were also improved from 510[%] to 7.9[%], and it was found that the waveform

became closer to a sine wave, providing excellent quality input current. It was confirmed that the speed response characteristic was excellent according to the change of the driving situation in the high-speed range. When a load was applied during steady-state operation in the medium speed range, the stabilization interval of the current in the presented method was delayed by 0.5 seconds compared to the existing 0.2 seconds. When a reverse speed command was applied during steady state operation in the low speed range, it was confirmed that both methods were stably controlled within 0.2 seconds.

The presented power conversion system is expected to be used as an emergency operation method in the electric propulsion of small ships with space constraints, such as fishing boats and leisure boats.

References

- Abu-Rub H(2012). High performance control of AC drives with MATLAB/Simulink models. Wiley, 400~403
- Hur JJ(2020). A study on the speed control ship propulsion induction motor using improved AFE rectifier, J korean Soc Fish Ocean Technol, 56(1), 71~81.
<https://doi.org/10.3796/KSFOT.2020.56.1.071>
- Hur JJ(2020). A Study on Speed Control Method of Propulsion Motor for Small Ships with AFE Converter. Jurnal of fishries and marine sciences education, 32(1), 49~64.
<https://doi.org/10.13000/JFMSE.2020.2.32.1.49>
- Hur JJ, Kang KW, Kim JS and Kim SH(2018), Speed control for direct current motor using an AFE rectifier, Journal of the Korean Society of Marine Engineering, 42(10), 892~836.
<https://doi.org/10.5916/jkosme.2018.42.10.829>
- Hur JJ, Kim YJ, Yoon KK, Oh SG, Noh JH, Kim SW and Kim JS(2021). A study on sensorless

- control of low-speed range for induction motors. *Journal of the Korean Society of Marine Engineering*, 45(2), 79~87.
<https://doi.org/10.5916/jamet.2021.45.2.79>
- Jeong BH, Kim SK, Park JK, Oh GK, Cho GB and Baek HJ(2003). A study of using optimal hysteresis band amplitude for direct torque control of induction motor. *Power electronics conference*, 812~815
- Kim JH, Lee SS, Kim RY and Hyun DS(2012). A sensorless control using extended kalman filter for an IPM synchronous motor based on an extended rotor flux. in *Proc. 38th Annu. Conf. IEEE. Ind.*, 1631~1636.
<https://doi.org/10.1109/IECON.2012.6388731>
- Kim SH(2016). *Motor control - DC, AC, BLDC*. 2nd Edition. Bukdu PRESS. 114~140.
- Lee KB, Song JH, Choy I, Choi JY, Yoon JH and Lee SH(2000). Torque ripple reduction in DTC of induction motor driven by 3-level inverter with low switching frequency. *IEEE 31st Annual power electronics specialists conference*, 448~453.
<https://doi.org/10.1109/PESC.2000.878900>
- Steinke JK(1999). Use of an LC filter to achieve a motor-friendly performance of the PWM voltage source inverter. *IEEE Trans. Energy convers*, 14(3), 649~654.
<https://doi.org/10.1109/60.790930>
- Wlas M, Krzeminski Z, Guzinski J and Abu-Rub H(2005). Artificial-neural-network-based sensorless nonlinear control of induction motors. *IEEE Trans.* 20(3), 520~528.
<https://doi.org/10.1109/TEC.2005.847984>
- Yu Y, Huang S and Wang B(2018). Speed-sensorless vector control with single phase current sensor for induction motor drives using current compensation method. *21st ICEMS*, 1590~1594.
<https://doi.org/10.23919/ICEMS.2018.8549135>
-
- Received : 24 September, 2021
 - Revised : 08 November, 2021
 - Accepted : 11 November, 2021